

## Article

# Analysis of Physicochemical Properties of W1.8507 Steel Parts with Sharp Edges, Thermochemically Treated by Plasma Nitriding with and without Polarized Screens

Mihai Axinte <sup>1</sup>, Petrica Vizureanu <sup>1</sup>, Nicanor Cimpoesu <sup>1</sup>, Carmen Nejneru <sup>1,\*</sup>,  
Diana-Petronela Burduhos-Nergis <sup>1,\*</sup> and Elena-Luiza Epure <sup>2</sup>

<sup>1</sup> Faculty of Materials Science and Engineering, Gheorghe Asachi Technical University, 700050 Iasi, Romania

<sup>2</sup> Department of Natural and Synthetic Polymers, Faculty of Chemical Engineering and Environmental Protection, Gheorghe Asachi Technical University of Iasi, Str. Prof.dr.doc. D. Mangeron nr. 73, 700050 Iasi, Romania

\* Correspondence: carmen.nejneru@academic.tuiasi.ro (C.N.); burduhosndiana@yahoo.com (D.-P.B.-N.)

**Abstract:** The plasma nitriding edge effect phenomenon is characteristic of parts with sharp edges. The intersection for the discharge of negative light of the two adjacent faces causes the apparition of this effect. In some cases, this effect causes disturbance to the general process. In this work, a sample with different angles of 30°, 60°, and 90° was analyzed. The sample was subjected to ion nitriding with and without the cathode grid to highlight the reduction of the edge effect on the non-uniformity appearing on the edges and corners of the parts. The effect of the active screen was also analyzed by hardness measurements in the area of the nitride edges and by SEM and EDX analyses in the mentioned areas. Additionally, the influence of active screens was studied by nanoindentation and scratch tests and by measuring the contact angle of coolants and liquid lubricants on the nitride surfaces with both methods.

**Keywords:** active screen plasma nitriding; edge effect; contact angle; negative glow discharge



**Citation:** Axinte, M.; Vizureanu, P.; Cimpoesu, N.; Nejneru, C.; Burduhos-Nergis, D.-P.; Epure, E.-L. Analysis of Physicochemical Properties of W1.8507 Steel Parts with Sharp Edges, Thermochemically Treated by Plasma Nitriding with and without Polarized Screens. *Coatings* **2023**, *13*, 177. <https://doi.org/10.3390/coatings13010177>

Academic Editor: Michal Kulka

Received: 14 December 2022

Revised: 2 January 2023

Accepted: 10 January 2023

Published: 13 January 2023



**Copyright:** © 2023 by the authors. Licensee MDPI, Basel, Switzerland. This article is an open access article distributed under the terms and conditions of the Creative Commons Attribution (CC BY) license (<https://creativecommons.org/licenses/by/4.0/>).

## 1. Introduction

Plasma nitriding or ionic nitriding technology is well-established. Due to numerous dependent technological parameters: pressure, electrode voltage, temperature, gas percentage, and the working atmosphere dissociation degree, technology presents certain difficulties in terms of controlling negative phenomena. These are the double cathode effect, the edge effect, and the electric arc occurrences risk. This unwanted phenomenon produces local energy in high concentrations and differences in temperature on the part surfaces. It results in a heterogeneous diffusion layer and occurrences of white layers, chemical compounds, or, in certain cases, even scrapping the part surface by local melting [1]. Intense physical pulverization represents another disadvantage of plasma nitriding. This is produced by applying the plasma discharge directly on the parts' surface. Two phenomena are produced: first, the reactivity is improved, but, at the same time, the surface quality decreases due to increased roughness and the appearance of an exfoliation area.

In Ref. [1], plasma nitriding technology is characterized by these disadvantages, which force numerous restrictions on this technology. Among these restrictions, the following are mentioned: the complexity of the parts, the placement of many parts with various geometries on the cathode working table, temperature, electric field distribution, the obligation to chemically clean the surfaces, and the elimination of sharp edges, peaks, or any roughnesses that can favor an electric arc.

Active screen nitriding is a technology that largely solves the difficulties of classical plasma nitriding. In other studies in the field, the term active screen can also be found in the form of a cathode grid or polarized screen. The principle behind this technique is to

modify the geometry of the electric field between electrodes: the anode and the cathode. This is carried out by inserting another electrode, an active or neutral metal screen, between the anode and the cathode between space. Plasma discharge is mediated through the grid and is no longer produced directly on the part, obtaining better uniformity of the electric field on the part surface. As a result of this method, the negative effects caused by cathodic discharge events directly on the part, and the local concentration that results from accidentally discharging arc energy, are reduced.

In the plasma nitriding process, the treated parts are connected to high cathodic voltages, and the plasma acts directly on the surface of the parts. Electric field distortions in parts with more complex geometry occur around sharp edges. This is called the edge effect. This effect is produced when cathodic discharge is applied to wall intersections. In those areas, the combined discharge effect from the intersecting walls creates a high energy concentration leading to different nitriding conditions compared to the plain wall conditions. This effect is present, for example, at the edges of the parts, as in Figure 1. The samples showing these edge effects show restriction rings (erosion rings) characterized by the strong variation of the hardness and thickness for the nitrided layer. These defects are more pronounced in steels containing alloying elements such as Cr and Mo, making it impossible to apply the plasma nitriding process to certain products such as knives, springs, molds, and tools where a high degree of uniformity of the superficial mechanical properties is required. In the case of mild steels such as AISI 1020, these defects are less pronounced [2].

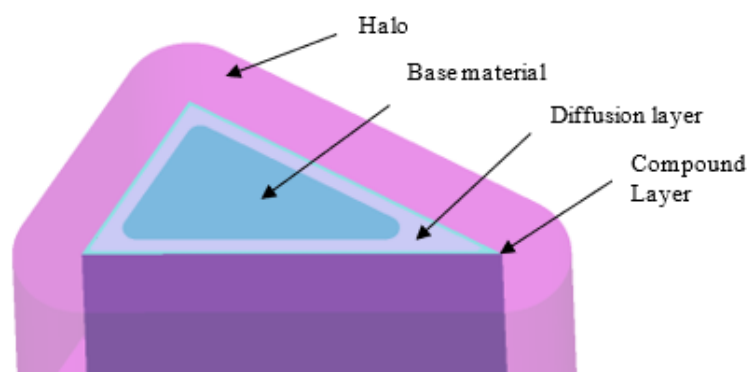


**Figure 1.** Illustration of the edge effect mechanism.

Khan et al. studied the active screen effect by observing the physicochemical characteristics of nitrogen diffusion layers obtained with and without an active screen. Both active screen plasma nitriding and DC plasma nitriding increase microhardness, but the active screen plasma nitriding increase is about three times greater than the DC plasma nitriding increase. This study examines the use of the “sputtering and recondensation” model in active screen plasma nitriding using metallurgical and optical emission spectroscopy analysis [3].

Additionally, Hassani-Gangaraj and Guagliano [4] developed a model of the inner and outer edge effect that predicts the appearance of layers of various types of nitrides [4].

Haftlang et al. [5] investigated the method by which an improvement in the electrochemical behavior of AISI 1045 steel could be achieved after applying aluminum nitride coating in 3.5% NaCl solution using potentiodynamic polarization and electrochemical impedance spectroscopy (EIS) analysis [5]. At the same time, Wang et al. [6] studied the effect of nitriding treatment in plasma with an active screen, observing the fact that results showed that the thickness of the nitride layer could be significantly improved using low gas pressure; the thickest layer of nitride layer was obtained at a gas pressure of 100 Pa. Additionally, a favorable single S-phase microstructure without chromium nitrides precipitation in the nitride layers was formed during rapid D.C. plasma nitriding at low

gas pressure. The possible mechanism was determined as the appropriate gas pressure at which the cathodic ion bombardment might favor the nitriding efficiency [6].

The authors Hosseini and Ashrafizadeh [7] carried out a paper that presents methods for determining the thickness of the nitrogen diffusion layer in Fe depending on the plasma parameters used characterized by glow discharge optical emission spectroscopy (GDOES) and secondary ion mass spectroscopy (SIMS), respectively. Nitrogen diffusion depths were accurately determined by optical and scanning electron microscopy at various nitriding durations. There was a clear correlation between SIMS data and microscopic evaluations for various nitriding cycles. After 10 h of plasma nitriding at 550 °C, SIMS reports that nitrogen diffusion depths of roughly 2000 nm were discovered in the diffusion zone. Previous examinations using traditional techniques, such as EDS, GDS, XPS, EPMA, or ion sample techniques, have not discovered such high depth [7].

Asadi and Mahboubi [8] investigated the properties of the nitrided substrates by evaluating the compound layer thickness, case depth, phase composition, and hardness profile. Both methods showed increased compound layer thickness, hardness, and nitrided case depth with increasing groove width. Additionally, in each sample, nitrogen atoms penetrated more deeply into the regions of the groove closer to the edge. A hollow cathode effect occurred in the sample with a 2 mm width groove when employing the CPN method, leading to the overheating of the sample.

In ref. [8], the influence of the hydrogen concentration in the plasma used for the nitriding of cavity-resistant steels was studied by Allenstein et al. [9]. The data presented in this study show that the phases' formation and distribution on the nitrided layer are significantly influenced by the gas mixture nitrogen content. Additionally, for the samples treated at 5% N<sub>2</sub>, better cavitation erosion resistance was signaled due to the finer and more homogeneous distribution of the nitride layer phases. Otherwise, worse cavitation erosion behavior for samples nitrided at 20% N<sub>2</sub> is supposed to be due to the formation of a multiphase compound layer constituted by Fe<sub>4</sub>N + Fe<sub>2</sub>-3N + CrN, which can infer residual stress in the treated surface [9].

The double cathode effect was analyzed by Shen et al. [10] on the thermochemical treatment of AISI 304 austenitic stainless steel assisted by two coaxial cylinders. Since the coaxial cylinders instead of treated samples were subject to high cathodic potential, the inherent shortcomings of the conventional D.C. technique were eliminated. Additionally, the study shows that the higher temperature and defects caused by the cathodic ion bombardment might favor the nitriding efficiency of samples nitrided on cathodic potential.

The analysis of the plasma nitriding of the welded parts was carried out by Alphonsa et al. [11], showing that welded joints using the multiple-pass technique provided better nitriding properties compared with those of the single-pass technique. An improvement in the hardness was also observed by three times which could be correlated with structural changes and process parameters.

Researchers Naeem et al. [12] studied the effect of the variation of the diameter of the cathodic cage effect of cathodic cage size on plasma nitriding of AISI 304 steel on the structure and some physicochemical properties of the plasma nitrided layers of AISI 304 steel.

The analysis of nitrogen diffusion in the plasma layer in the Fe Armco alloy was carried out by Jasinski et al. [13]. The migration of the nitrogen atoms' uphill diffusion effect was observed, which confirmed the migration of the atoms in the diffusive layer towards the top surface ( $\epsilon/\epsilon + \gamma'$  interface) and stress change effect in the nitrogen saturation area of the (Fe(C, N) +  $\gamma'$ ) layer.

Additionally, Bracerasa et al. [14] studied the effect of ionic nitriding inside AISI316L steel tubes. The conclusion of this study shows that a relationship was established between plasma treatment parameters, geometrical features, and corrosion resistance, with corrosion resistance preservation and improved tribological performance, while ECR monitoring was found to be insightful and informative of the evolution of the latter.

Researchers Kajzer et al. [15] studied the characteristics of the contact angle of water and some biological liquids on nitrided and nitrocarburized surfaces; we obtained the same wetting characteristics.

In this work, the authors Borgioli et al. [16] studied the effect of changing the roughness through the polishing of nitrided parts made of AISI 202 steel on the contact angle achieved by distilled water and the effect of grinding on the corrosion of the nitrided layer.

Taking into account all the studies discussed so far, the need to perform an experimental analysis of the efficiency of the cathodic screen in reducing the crowding effect that occurs during ionic nitriding as well as how the cathodic screen helps to obtain a better surface quality for the nitrided sample is observed.

As a novelty, we can mention the fact that in this paper, correlations were made between comparative contact angle studies on the grid and non-grid nitrided surfaces with standard and industrial liquids and scratch and nanoindentation studies for the comparative determination of the physical properties of nitrogen deposits through the two methods.

## 2. Materials and Methods

In this study, plasma nitriding was studied with an active screen to reduce the edge effect. This was highlighted by comparing the properties of the edges of the nitrided layers on the sample specially built for this scope. The experimental installation is presented in Figure 2.

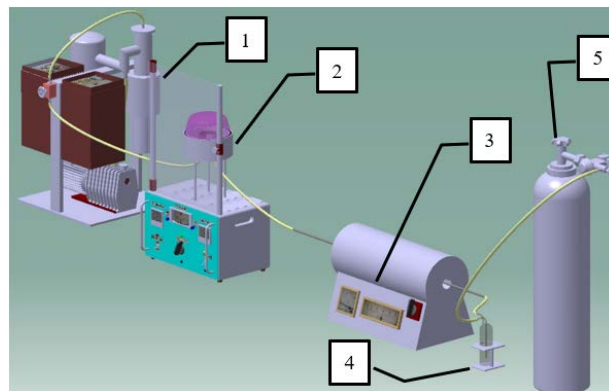


**Figure 2.** Principle diagram of the experimental installation used for nitriding: (1) vacuum pump, (2) nitriding installation, (3) ammonia dissociation furnace, (4) flow meter, and (5) ammonia gas tank.

This study used samples made of different types of steel (W1.8507) as substrates. The semi-finished product from which we made the samples was subjected to martensitic tempering and high-tempering treatments. The W1.8507 steel specimens' chemical composition was determined by the Foundry Master spectrometer and is presented in Table 1.

**Table 1.** Chemical composition of W1.8507 steel.

Element	Fe	C	Cr	S	Mo	Ni	Al	Cu	W	Ti
%wt.	balance	0.403	1.37	0.029	0.157	0.122	1.07	0.122	0.065	0.016

To analyze the effect of the polarized screen on the sharp edges of the pieces, we used a sample in the shape of a triangular prism. A 10 mm diameter base cylindrical sample was used. A triangular prismatic upper sample was produced by milling the upper part at 30, 60, and 90 degrees. Using an anode with a diameter of 200 mm, tests were conducted without polarized screens (Figure 3a,c) and with polarized screens (Figure 3b,d), represented by cathode polarized screens with a diameter of 65 mm. Figure 3a–c and d show the formation of the electric discharge field around the interior and exterior angles.



SEM microscopy (Tescan, Brno, Czech Republic), EDX chemical analysis (Bruker/Roentec Co., Berlin, Germany), and microhardness tests (Bruker, Ettlingen, Germany) were used on the metallographic components to examine the treated samples.

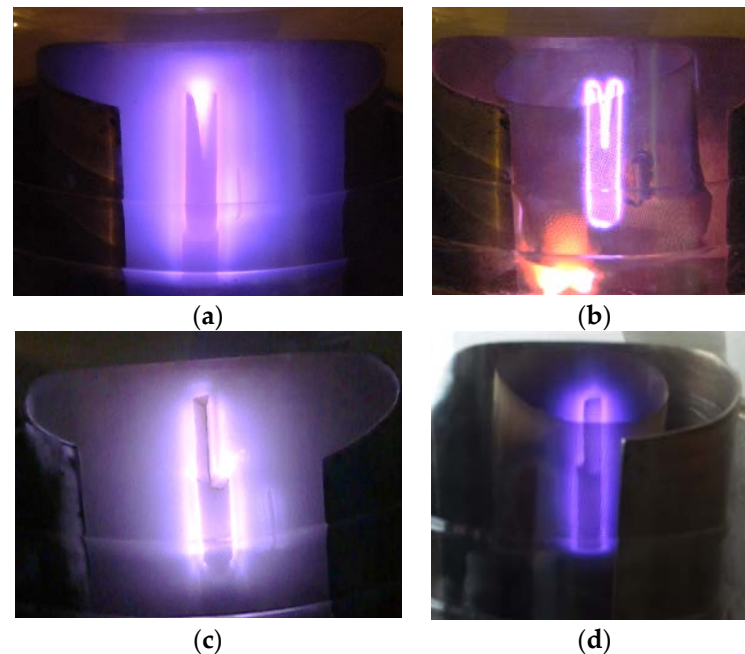


**Figure 3.** Images of the nitriding enclosure. Sample with interior angles: (a) no screen nitriding, and (b) active screen nitriding. Sample with exterior angles: (c) no screen nitriding and (d) active screen nitriding.

The parameters of the discharge regime for the two types of treatments are presented in Table 2.

**Table 2.** Working parameters of the nitriding process.

	T [°C]	P [torr]	$U_k$ [V]	$I_k$ [A]	$I_g$ [A]	t [h]
No screen	500	1	480	0.1	-	7
With screen	500	2	470	0.18	0.04	7

Where:  $U_k$  = Cathodic voltage, in [V];  $I_k$  = Cathodic intensity, in [A];  $I_g$  = active screen intensity, in [A].

To analyze the wettability of the flat surfaces, we inspected the static contact angles of the liquid droplets on the samples with the Drop Shape Analysis software (DSA version 1.90.0.14) of the Kruss Easy Drop goniometer. Before the measurements, the surfaces of the samples were cleaned with detergent, rinsed with distilled water and pure ethanol, and then equilibrated under ambient conditions overnight. The contact angle measurements were performed with distilled water, ethylene glycol, purity 96%–98%, cooling liquid (emulsion), and anti-friction oil.

Depending on the testing liquid, standard or technical, stainless steel needles with a diameter of 0.5 and 1 mm, respectively, were used. Each measurement was conducted for 40 s every 2 s. The first 10 s were not taken into account because it was found that in this interval, the thermodynamic balancing of the drop on the surface takes place. Calculating the average of the contact angle data was followed by comparing each value's departure from the average. Values with a variation of 5° were excluded. A new average was created using the remaining results, which served as the basis for future analysis of the contact angle value. It should be noted that the new average and the error bar were calculated for a minimum of six values.

The microindentation and scratch tests were conducted on a CETR UMT-2 microtribometer (Bruker, Ettlingen, Germany), and the test conditions were as follows:

(1) During the micro indentation test, a Rockwell-type indenter (diamond cone with an angle of  $120^\circ$  and a radius tip of 200 microns) was used. The samples were fixed on the table and were pressed with a vertical force of 10 N: preloading time 15 s, loading time 30 s, holding time 15 s, and unloading time 30 s. The software performed the automatic test and recorded the vertical load  $F_z$ , time, and vertical travel distance  $C$  of the indenter.

(2) For the scratch test, an Nvidia cutting blade with a radius at the tip of 0.4 mm was used. The samples were fixed on the table, and during the test, the samples were pressed with a vertical force of 10 N, moving the table over a distance of 10 mm in 60 s, and the test speed was 0.167 mm/s. The software performed the automatic test and recorded the vertical force  $F_z$ , horizontal force  $F_x$ , acoustic emission signal AE, and time and distance of movement in the horizontal direction  $Y$ .

### 3. Results and Discussion

#### 3.1. SEM and EDX Plasma Nitrided Layers Analysis from Prismatic Samples

We conducted section analyses on characteristic areas at the angles of 30, 60, and 90, as well as on the sides. This was carried out to examine the effect of the polarized screen on the sharp edges and structural changes at the level of the thin outer layers. The sample used for the experiment is shown in Figure 4a.

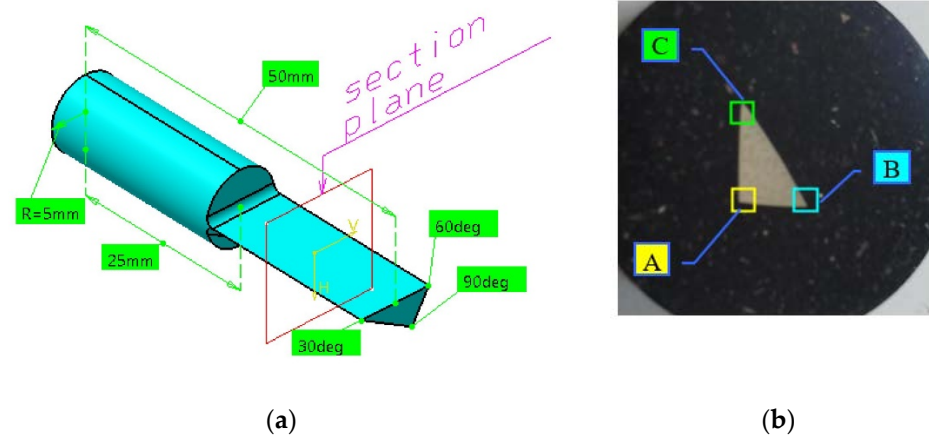


**Figure 4.** Sequence for obtaining the micrograph samples: (a) sample used for experiment with sectioning plane and (b) embedded sample.

To perform the microstructural analysis of the outer layer of the sample, we proceeded to section it. We made the sectioning of the sample perpendicular to the vertical edges of the right triangular prism (Figure 4b). We performed morphological analyses using the microscope in the areas indicated in Figure 4b.

The SEM images are presented successively in the following order: Figures 5–7 are for the nitrided sample without the polarized screen, and Figures 8–10 represent the nitrided sample with the polarized screen. The most visible irregularities are found in the edge and corner areas (Figures 5–7). The chemical compositions are presented in the tables attached to the figures.

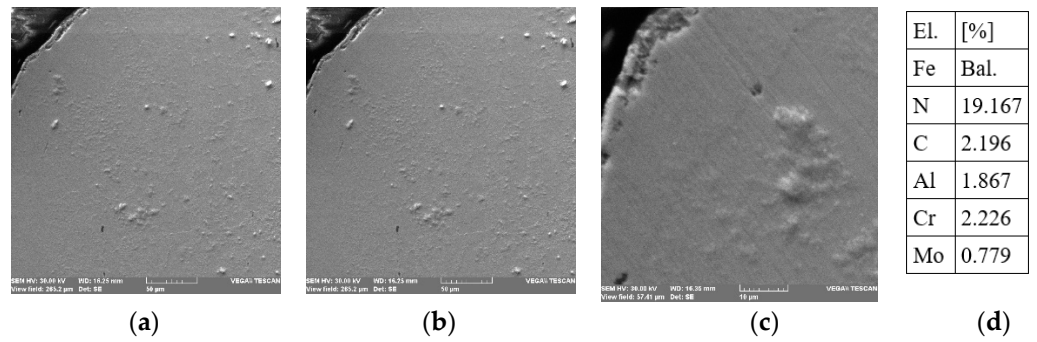


Figure 5. No screen nitrided sample SEM micrographs, 90° area A, different scale: (a) 50 μm, (b) 20 μm, (c) 10 μm, and (d) mass concentration of elements per area.

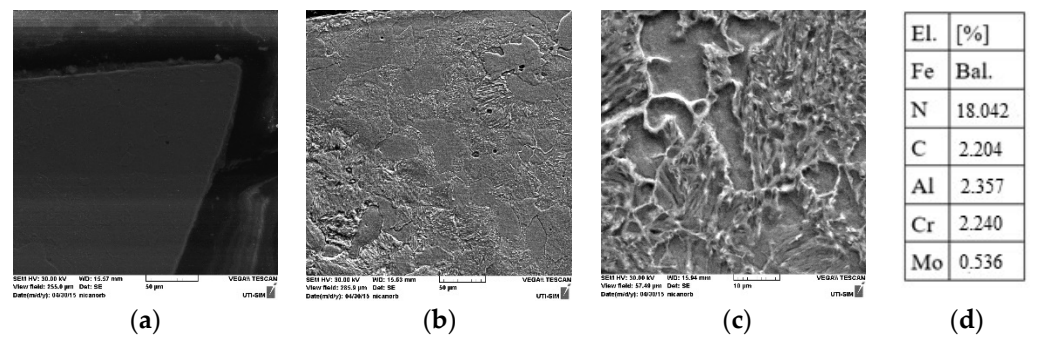


Figure 6. No screen nitrided sample SEM micrographs, 60° area B, different scale: (a) 50 μm, (b) 50 μm, (c) 10 μm, and (d) mass concentration of elements per area.

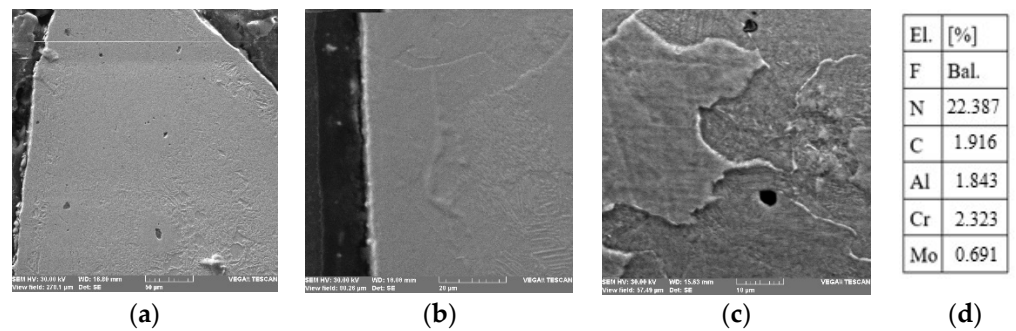


Figure 7. No screen nitrided sample SEM micrographs, 30° area C, different scale: (a) 50 μm, (b) 20 μm, (c) 10 μm, and (d) mass concentration of elements per area.

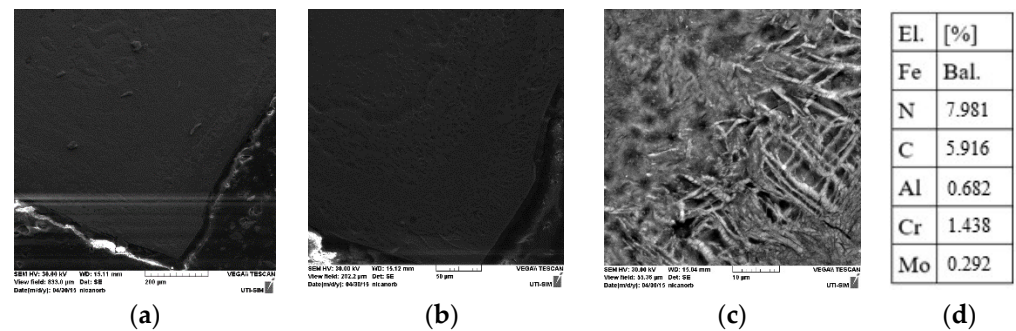


Figure 8. Active screen nitrided sample SEM micrographs, 90° area A, different scale: (a) 200 μm, (b) 50 μm, (c) 10 μm, and (d) mass concentration of elements per area.



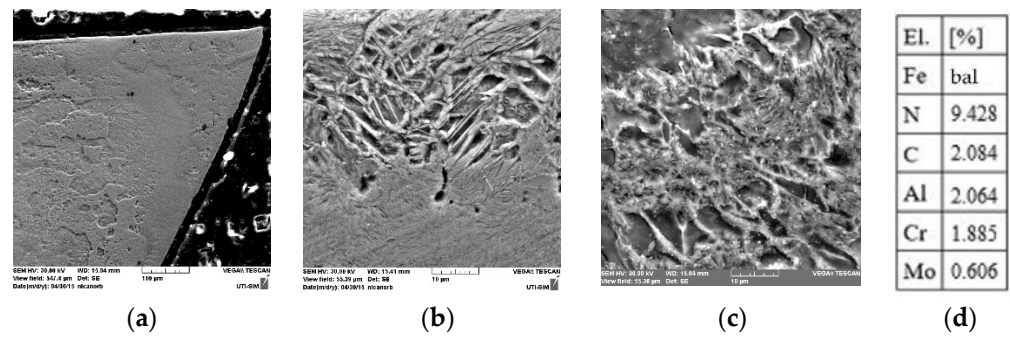


Figure 9. Active screen nitrided sample SEM micrographs, 60° area B, different scale: (a) 100 μm, (b) 10 μm, (c) 10 μm, and (d) mass concentration of elements per area.

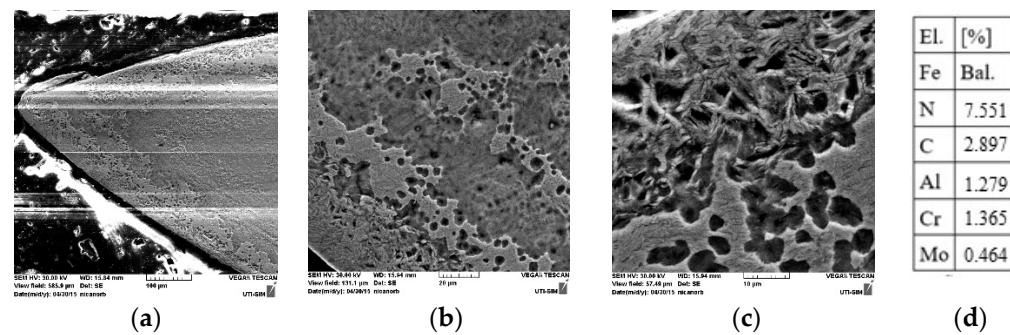
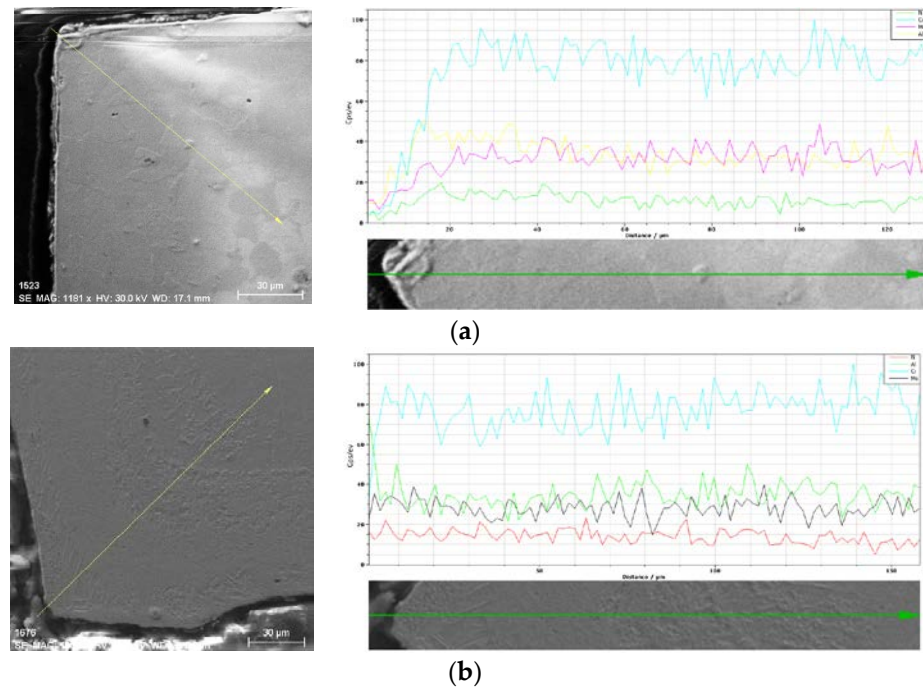


Figure 10. Active screen nitrided sample SEM micrographs, 30° area C, different scale: (a) 100 μm, (b) 20 μm, (c) 10 μm, and (d) mass concentration of elements per area.

Figure 11 shows the line analysis of the sample at a 90° angle. Figure 11a shows the sample without a polarized screen, and Figure 11b shows it with a polarized screen. Studying the SEM photos, we can observe that the nitrogen absorption at the edge of the part is more uniform for active screens compared to no-screen technology. The concentration of nitrogen in the no screen plasma nitride sample is rather small for the first 10 μm, as shown in Figure 11a green line. However, for active screen plasma nitriding, the nitrogen concentration is rather stable for all the line analyses.

The use of the active screen has a positive effect on the surface of the treated part, and the treated surface has a low number of surface defects as different adhesions, roughnesses, exfoliation, and unevenness of the formed layer, as can be seen by comparing Figure 12a–d for no screen nitriding with Figure 13a–d when nitriding with a screen.

The SEM figures of the microstructure show that the thickness of the diffusion layer is relatively uniform for the active screen, unlike the case of the no-screen nitriding treatment when the areas with sharp edges present a thickening of the diffusion layer in contrast with the adjacent areas, where we can observe a thinner layer. This is possible due to the polarized screen protection against electric arcing. This could lead to local overheating and defects caused by microdrills of the parts. This phenomenon, in the absence of the active screen, could modify the diffusion parameters.



**Figure 11.** Chemical element distribution for N, Al, Cr, and Mo, and line analysis, for 90° area, after plasma nitriding: (a) no screen and (b) with a polarized screen.

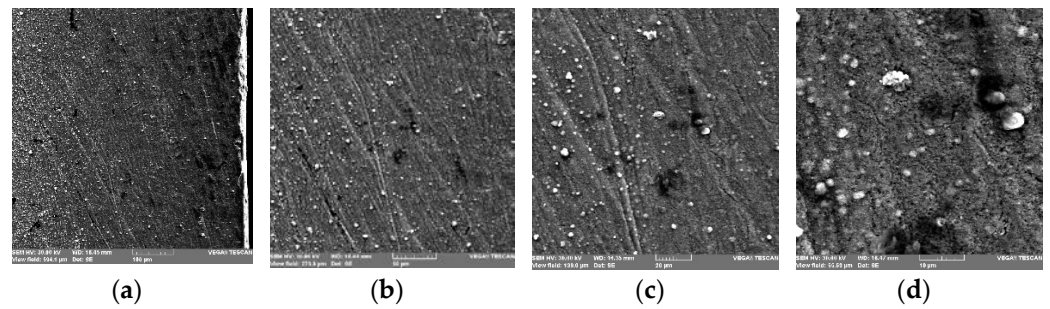


**Figure 12.** Microstructures of the ionic nitrided structure without the polarized screen, in the area adjacent to the 30° edge, at the top of the prismatic section, and a distance of 40 mm from the base of the part. SEM images at different magnifications: (a) 500×, (b) 1000×, (c) 2000×, and (d) 5000×.

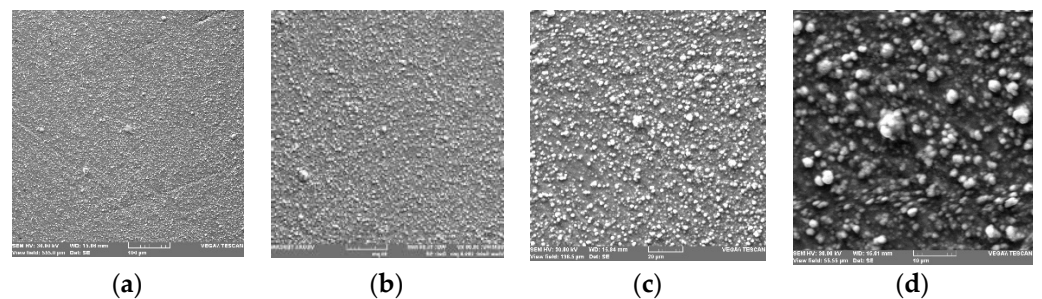


**Figure 13.** Microstructures of the ionic nitrided structure with the polarized screen—the 30° edge area at the top of the prismatic section and a distance of 40 mm from the base of the part. SEM images at different magnifications: (a) 500×, (b) 1000×, (c) 2000×, and (d) 5000×.



Analysis of the SEM images of the samples nitrided in plasma, without a polarized screen (Figure 12a–d), shows the presence of significant irregularities (adhesions, rough surface, micro craters, and micropumps). This is due to the phenomenon of intense physical sputtering that creates rough surfaces.

The surface SEM analysis for the layer deposited by ion nitriding without the grid (Figure 12a–d) and with the grid (Figure 13a–d) highlights the surface quality of the deposited layer. The use of the polarized grid has a positive effect on the roughness; the resulting surface has a relatively small number of apparent defects of the following types: adhesions, roughness, exfoliation, and non-uniformity of the deposition, compared to Figure 12. It can be seen on the SEM photos of the sections (Figures 8–10) on the edge and corner areas that the formation of the coral-type surface layer is uniform and relatively compact.

Physical spraying produces better deposition quality because it applies to the entire surface evenly and with low intensity. Because a polarized screen surrounds the part, the electric field is uniformly distributed around the part during physical spraying. Throughout the surface of the part, the electric field is evenly distributed. The same amount of energy is spread over a larger surface, free from concentration on a sharp edge or corner area. The nitrogen diffuses deep inside the part due to the decrease in physical spraying and the increase in chemical spraying. Therefore, the edge effect is reduced, and uniform diffusivity is obtained.

EDX analysis of the prismatic sample treated without a polarized screen shows a fluctuating nitrogen concentration on the surface, between 18.04% and 22.39%, which is caused by the edge effect, which leads to a higher local absorption of nitrogen.

EDX analysis of the prismatic sample treated with a polarized screen indicates a fluctuating nitrogen concentration on the surface, between 3.47% and 8.09%. This is caused by the edge effect, which leads to reduced absorption of nitrogen.

The results confirm that nitriding without an active screen is prone to higher nitrogen local concentrations, but the surface quality is lower compared to an active screen due to bigger temperature variations and high physical spraying.

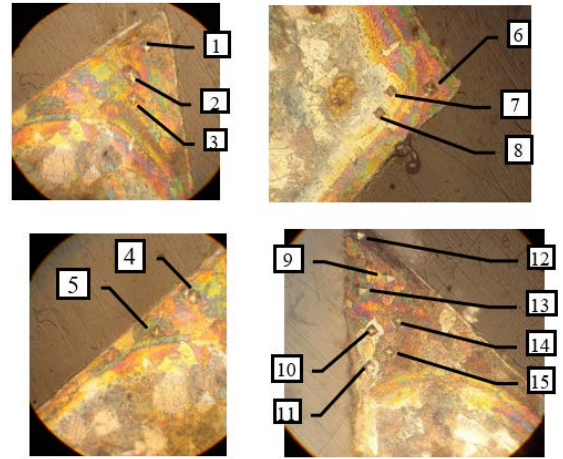
It can be seen that the grid effect on the surfaces adjacent to the edges is very strong, as demonstrated by the comparison of Figures 12a–d and 13a–d [8]. This can also be seen in the work carried out by Asadi and Mahboubi. The authors observed the effect of the cathodic grid to standardize the deposits on the surface, strongly mitigating the microcraters generated as a result of physical spraying.

### *3.2. The Microhardness of the Metallographic Constituents for No Screen Ionic Nitrided Sample*

For the microhardness analysis, measurements were carried out using the PMT3 microhardness meter. The pressure weight of the diamond penetrator had a mass of 50 g (HV50). The measurement of the microhardness on the section was carried out in the same areas as the SEM and EDX analyses, according to Figure 4b, areas A, B, and C, both for those nitrided with a screen and those nitrided without a screen. This was conducted to generate a comparison with the areas of the part nitrided using the polarized screen, where the plasma was formed without discontinuities and the occurrence of electric arcing and other undesirable phenomena. The results obtained when measuring the hardness are presented in Table 3.

**Table 3.** Microhardness values of the metallographic constituents in areas A, B, and C along with the images of the marks measured for the nitrated sample without a screen.

No.	HV	Metallographic Constituent	Zone
1	734.03	Ferrite	A
2	577.78	Ferrite	
3	551.95	Ferrite	
4	587.27	Pearlite	
5	734.03	Ferrite	
6	577.78	Pearlite	B
7	816.53	Ferrite	
8	700.00	Ferrite	
9	669.82	Ferrite	C
10	642.94	Ferrite	
11	587.27	Ferrite	
12	793.83	Ferrite	
13	734.03	Pearlite	
14	700.00	Pearlite	
15	734.03	Pearlite	



This effect leads to an increase in the temperature on the corners, something that influences mass transfer, uneven diffusion zones, and intense decarburization. The non-uniformity of the diffusion layer obtained in the corner areas can be seen in Table 3.

The microhardnesses measured on the edge areas show the presence of ferrite and allied pearlite but with moderate nitrogen content.

The microhardness measurement on the section was carried out in the same areas as in the ion nitrated specimen without a polarized screen, where the edge effect appeared on the edge generators and the top edges. This was conducted to compare areas of the nitrated part with the polarized screen where the plasma formed without discontinuity and without the appearance of arcing and other unwanted phenomena.

The microhardness measured on the edge areas shows the presence of ferrite and allied pearlite because the hardnesses, in the majority, are in the range of 551 HV50–816 HV50.

### 3.3. Microhardness of the Metallographic Constituents for Active Screen Ionic Nitrated Sample

The microhardness measured on the corners and edges has values mostly between 300 HV50–768 HV50, which indicates additional hardening of the layer due to the uniformity of the diffusion process.

It is observed that with the same type of diffusion, in the case of ionic nitriding with a polarized screen, a lower percentage of nitrogen is obtained on the surface, between 7.55% and 9.43%, implicitly a hardness with 15% to 20% reduced hardness, but with much better surface quality and higher uniformity of the microhardness properties. This is shown in Table 4.

On the corner and edge areas, the edge effect appears due to the intersection of negative lights and their input energies. The temperature on the corners rises as a result of this impact, which affects mass transmission and results in unequal diffusion zones and excessive decarburization. By comparison, it is simple to see the non-uniformity of the diffusion layer produced during nitriding without a polarized screen in the corner sections.

**Table 4.** Microhardness values of the metallographic constituents in areas A, B, and C along with the images of the marks measured for the ionic screen nitrided sample.

Zona A		Zona B	
No.	HV	No.	HV
1	316.49	10	416.53
2	316.49	11	372.59
3	300.00	12	440.83
4	369.82	13	651.60
5	372.59	14	681.30
6	416.53	15	671.60
7	525.00	16	661.20
8	671.60	17	494.88
9	716.33	18	765.05

Zona C	
No.	HV
26	366.53
27	475.00
28	366.53
29	475.00
30	580.46
31	390.83
32	507.46
33	621.60
34	666.33
35	715.05
36	768.27

Surface decarburization is favorable for nitriding. As a result of chemical spraying and temperatures around 600 °C, moderate decarburization results in the formation of chemical compounds of the CnHm type in the plasma volume. They create vacancies in the crystalline matrix, facilitating nitrogen atoms’ penetration into the metal matrix. On the other hand, classic nitriding, intensifies the physical spraying process in the edge areas and reduces chemical spraying. Therefore, the superficial decarburization process increases. This increases the risk of developing thin, brittle nitride lamellas that reduce the mechanical properties of the resultant layer.

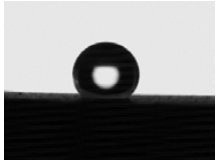
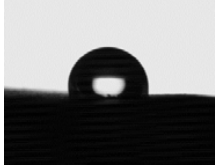
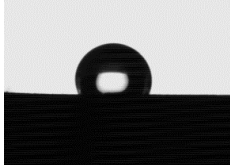
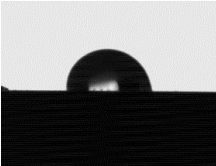
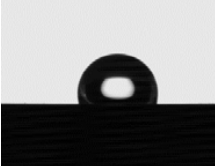
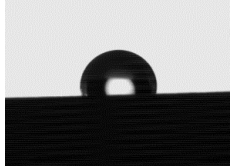
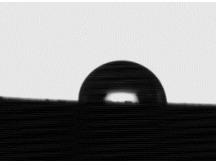
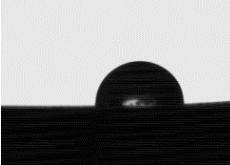
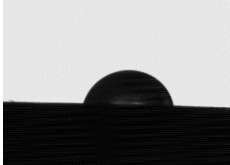
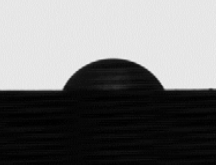
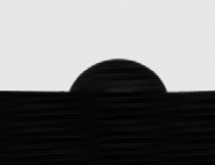
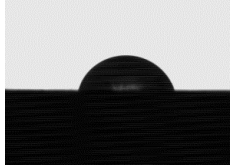
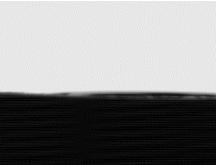
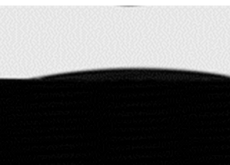
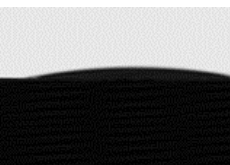
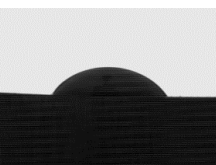
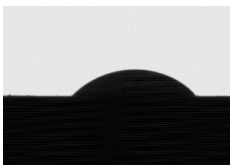
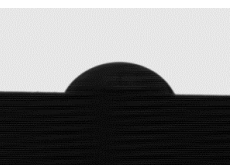
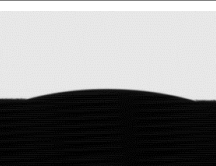
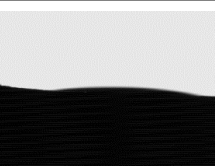
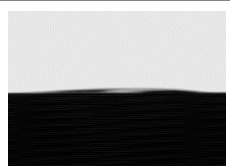


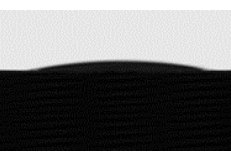
### 3.4. Contact Angle on Nitrided Surfaces with and without Polarized Screen

The contact angle when wetting with technical liquids on the surfaces of ion nitrided parts with and without polarized screen provides indications regarding the interaction between the surface with deposits and the various standard or industrial liquids with which it comes into contact during operation.

Ionic nitriding is mainly applied to two categories of parts: machining tools such as drills, broaches, disc cutters, and finger cutters and the second to moving transmission elements such as gears, transmission shafts, axles, or other bodies of rotation.

Two standard environments were used for the experiment, namely distilled water and ethylene glycol and two technical environments usually used in industrial applications, namely coolant (emulsion) used to remove chips from the results of mechanical processing operations and anti-friction oil used to lubricate the elements in motion. In Table 5, the images from the contact angle test are presented.

**Table 5.** Images obtained for contact angle test on nitrided surfaces.

Distilled Water			
	L Surface	X Surface	Y Surface
No screen			
With screen			
Ethylene glycol			
No screen			
With screen			
Cooling liquid			
No screen			
With screen			
Anti-friction oil			
No screen			
With screen			

The values obtained from the contact angles test are presented in Table 6 for no screen nitriding and Table 7 for active screen nitriding.

**Table 6.** The values of the contact angles on different angular surfaces and error bars in the brackets for samples nitrided in plasma without an active screen.

The Nitrided Side without the Active Screen	Standard Environments		Technical Work Environments	
	Distilled Water	Ethylene Glycol	Cooling Liquid	Antifriction Oil
L	124 (4.1)	92 (0.7)	6 (1.5)	12 (1.5)
X	103 (3.7)	89 (0.4)	5 (1.6)	9 (4.9)
Y	112 (2.1)	80 (0.6)	7 (0.69)	15 (0.1)

**Table 7.** The values of the contact angles on different angular surfaces and error bars in the brackets for the plasma nitrided samples with an active screen.

The Nitrided Side without an Active Screen	Standard Environments		Technical Work Environments	
	Distilled Water	Ethylene Glycol	Cooling Liquid	Antifriction Oil
L	87 (2.7)	67 (2.3)	45 (2.1)	5 (0.5)
X	97 (2.2)	67 (1.8)	44 (3.1)	7 (1.8)
Y	99 (2.6)	74 (2.1)	60 (4.8)	7 (0.9)

Where: L = the hypotenuse, X = the cathetus opposite the angle of 60°, and Y = the cathetus opposite the angle of 30°.

As shown in Table 6, the values of the contact angles obtained on different sides differ significantly in standard media such as distilled water and ethylene glycol.

Analyzing the contact angles, it can be seen that in the case of water, they are around 90° and 110°, respectively, indicating that the samples are hydrophobic. The values of the contact angle when the test liquid is ethylene glycol decrease compared to the values for water while maintaining the same tendency of non-spreading on the surface of the samples. These behaviors are correct, considering that the two liquids are polar. Hydrogen bonds between both water and ethylene glycol molecules are stronger than the physical interactions between the substrate and standard test liquids.

In the case of industrial environments, coolant and anti-friction oil, an opposite behavior is observed, spreading the liquids on the surfaces of the samples, meaning an oleophilic behavior.

The anti-friction oil provided contact angle values between 5°–7° on the nitrided surface with the grid and 9°–15° on the nitrided surface without the grid. This pronounced spreading of the oil favors the smearing of the samples. From a practical point of view, the oil that adheres more strongly to the surface of moving parts, such as shafts and gears, forms a boundary layer with the role of protecting the parts.

The data for the coolant are not awkward if we consider the practical application aspects. Spreading ethylene glycol on the nitrided part without the grid creates a liquid film that can be constituted as a relatively stable boundary layer on the nitrided part. The role of the coolant is also that of removing chips resulting from the use of nitrided chipping tools (drills, cutters, etc.). The boundary layer formed within the nitrided part without a grid could keep microchips near the tool edge, compromising surface quality and potentially leading to faster edge wear or chipping of the cutting edge. On active screen nitrided steels, the coolant forms contact angles in the range of 44°–60° signals, and does not produce good surface wetting, which is advantageous from a practical point of view as it helps to remove chips more quickly but is more efficient for cooling the support.

Studying the values from Tables 6 and 7, differences in the contact angles obtained on the three sides within the same sample can be observed. If we consider distilled water for analysis, it is found that for the nitrided sample without a grid, the maximum difference between the angle determined on the sides L and X is 21°, and in the case of the nitrided sample with a grid, the maximum difference, this time between Y and L,



is  $12^\circ$ . This suggests that the nitrided sample without a grid has a surface with more evident non-uniformities and a rougher surface at the micro/nanoscale. Nitrogen is more or less uniformly deposited on the surfaces during the nitriding process. This phenomenon, known as the edge effect, is also highlighted for the other test liquids, except for the coolant. With ethylene glycol as the nitrided part without the grid, we observed a maximum difference between the contact angles of  $12^\circ$  (the difference between the angle on the L side compared to the angle on the Y side), while for the nitrided samples with the grid, the maximum difference was  $7^\circ$  (between the angle on the L side and the angle on the Y side). The same trend was observed for the anti-friction oil, with the maximum difference between the angles for the nitrided sample with the grid being  $2^\circ$  and that for the nitrided sample without the grid being  $6^\circ$ .

The difference that appeared is due to the presence of the edge effect in the no-screen case when, on the edges of the sample, there is an intersection of plasma fields that generate non-uniformity of deposition.

The analysis of the effect of hydrophilicity and hydrophobicity of the surface of ionic nitrided steel with natural liquids was debated by researchers Kajder et al. [15] on ionic nitrided or nitrocarburized parts, but the effect was followed for Ringer type solutions, useful research in medical applications and not for industrial applications with classic liquids and industrial utility as in the present work. Even under these conditions, similarity of the effects can be observed for ethylene glycol and distilled water, which can be linked to the effects obtained with superficial deposits of nitrogen regardless of the final goal pursued.

### 3.5. Microindentation and Scratch Test of Nitride Samples with/without Active Screen

Figure 14 shows the typical loading–unloading curves of the experimental samples with and without a screen during the nitriding process from which the quantities such as the hardness (H) and indentation of Young’s modulus (E), among other mechanical properties, can be evaluated in Table 8. The values obtained for Young’s indentation modulus can be in small lines. This is different from Young’s modulus because it is a weighted average of the elastic properties in a certain sample volume, and Young’s modulus is directional. For isotropic materials, both values should be equal. In engineering sciences, Young’s modulus is used as a measure of the elastic properties of larger samples, which contain mostly a lot of differently oriented grains [17]. In the case of the nitrided sample, at least at the surface, the material is rich in nitrides from the surface (higher percentage) towards the inside of the sample concerning micrometer distances depending on the nitriding process parameters and treatment time. In this case, the experiments are set in the range of the nitriding depth with loads of 9N and maximum depths approximately  $6\ \mu\text{m}$ . The curve shape is similar to Figure 14 with a difference in the recovery part.

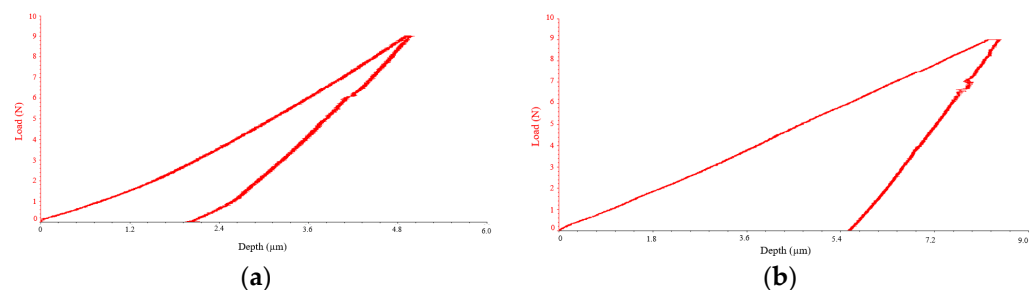


**Figure 14.** Indentation curves for samples nitride without (a) and with the grid in (b).

**Table 8.** The experimental result from micro indentation (three areas).

	No.	Indentation Young Modulus [GPa]	Hardness [Gpa]	Maximum Load [N]	Maximum Displacement [ $\mu\text{m}$ ]	Contact Stiffness [N/ $\mu\text{m}$ ]	Contact Depth [ $\mu\text{m}$ ]	Contact Area [ $\mu\text{m}^2$ ]
Sample nitride with grid	Point 1	96.33	8.92	9.00	8.48	3.27	6.42	1008.89
	Point 2	122.51	13.27	9.01	7.29	3.34	5.26	678.92
	Point 3	118.04	12.74	9.00	7.42	3.30	5.37	706.65
	Average	112.29	11.64	9.03	7.73	3.30	5.68	798.16
Sample nitride without grid	Point 1	238.01	38.83	9.01	5.02	3.47	3.07	231.89
	Point 2	251.55	37.34	9.00	4.96	3.70	3.14	241.08
	Point 3	237.84	41.91	9.03	4.99	3.34	2.97	215.49
	Average	242.46	39.36	9.01	4.99	3.51	3.06	229.49

Compared to Martens hardness, indentation hardness is a measure of the material response to permanent deformation or damage. For perfectly controlled experimental conditions, both determinations should provide the same values as conventional Berkovich (or Vickers) hardness methods. The big differences between the hardness values of the samples are based on the degree of nitriding reached by each sample during the process and the effect of the grid on the surface properties. To obtain similar hardness, the process with the grid can be maintained longer, and the surfaces will present similar values of surface hardness [18].

Based on the hardness differences, all the other properties present similar variations with a smaller contact depth or displacement for the harder sample. The contact stiffness is similar for both samples presenting a surface layer with homogeneous properties for the sample nitrated with the grid.

Progressive scratch revealed similar behaviors to  $F_x$  (horizontal force response of the material, Figure 15a), COF (friction coefficient, Figure 15b), and AE (acoustic emission, Figure 15c) for both samples. These variations were expected based on the nitriding progress from the surface along the nitrated depth. In the first 25–30 s of the experiment, the friction coefficient was similar for both samples.

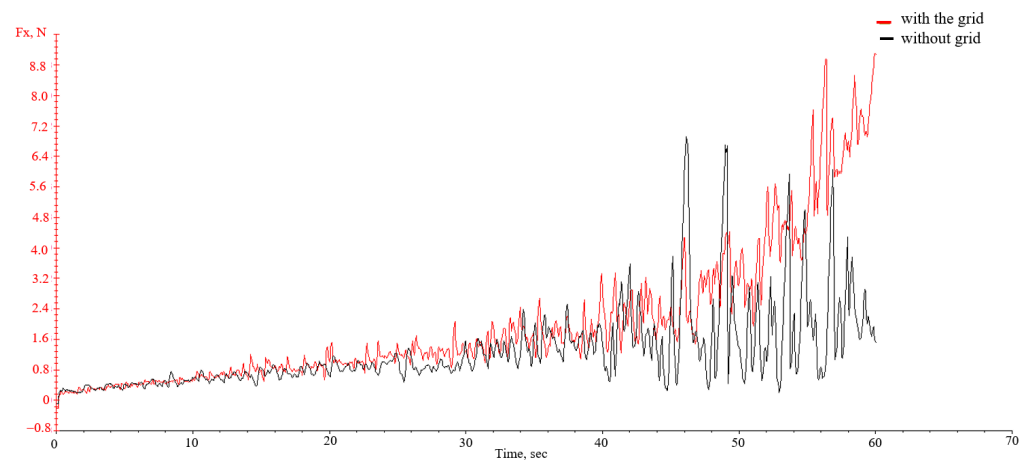
The acoustic emission of both surfaces is based on approximately same chemical composition and nature. The friction coefficient values, shown in Table 9, confirm the hardness of the surface with a higher value of the no-grid nitrated sample.

**Table 9.** Experimental result for the scratch test.

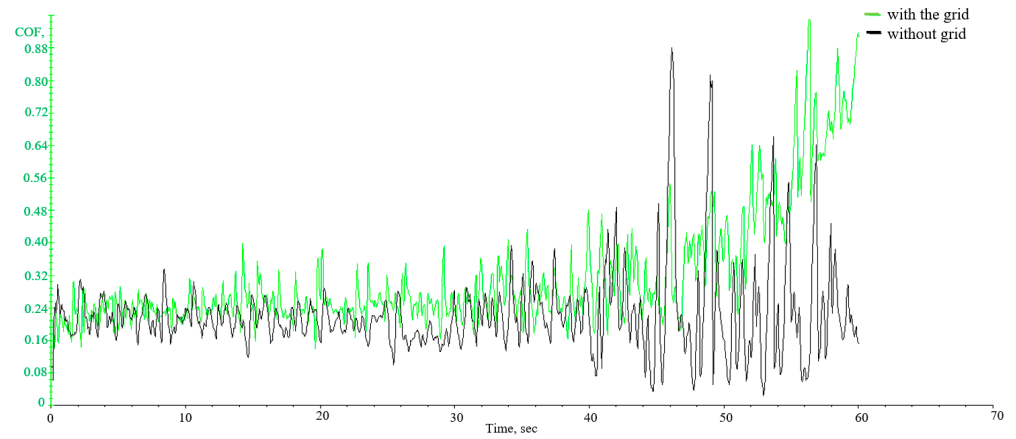
Material	$F_x$ [N] Average	AE [Volt] Average	COF Average
Nitrated with grid	2.01	0.02	0.32
Nitrated without grid	1.26	0.01	0.22

St.dev. (from 3 determinations):  $F_x$ :  $\pm 0.1$ ; AE:  $\pm 0.01$  and COF:  $\pm 0.05$ .

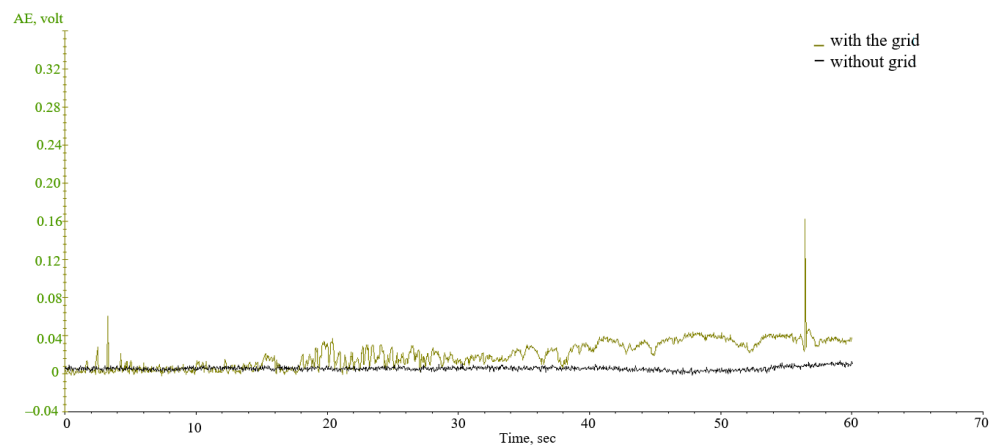
As determined by the scanning electron microscopy analysis of the scratch marks, no tensile or angular cracks were observed, as shown in Figure 16a. Surface contamination in the nitriding process without a grid is also highlighted in the SEM images shown in Figure 16. In addition to N enrichment of the surface, an oxidation process of the surface was observed. The 3D images of the scratch marks, shown in Figure 16b, present a double mark for the 3D profile of the scratch for the nitrated sample without a grid, which is caused by the variations of the surface hardness. These big differences were confirmed by the indentation test, as seen in Table 8 between points 2 and 3. Additionally, the depth of the mark was between 1, 2, and 4  $\mu\text{m}$ . Chemical composition insights were taken from selected points from Figure 16a.



(a)



(b)



(c)

**Figure 15.** Time variation of  $F_x$  (a), COF (b), and AE (c) during the scratch test for both cases of nitriding (with and without grid).

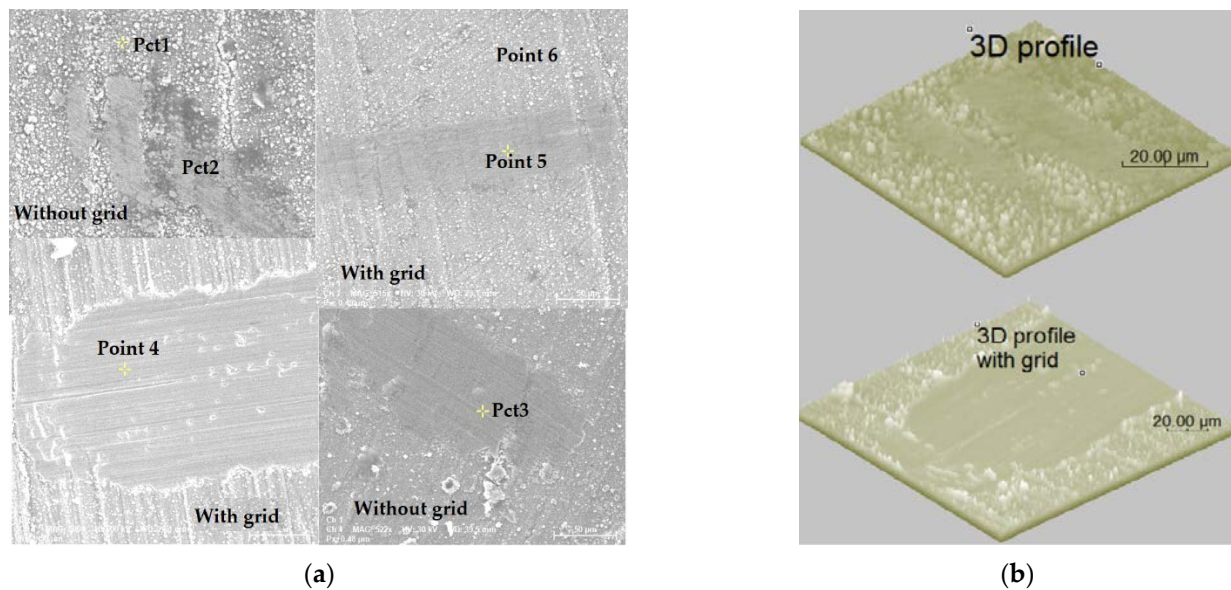


**Figure 16.** SEM images of the scratch mark on the nitride surface without and with grid and selected areas for the point mode chemical composition (automatic EDS detector). (a) SEM micrograph of scratch track profile; (b) 3d profile.

The tensile stress field developed by the indenter equipment tip causes tensile microfissures and cracks; furthermore, the displacement of the indenter tip usually provokes cracks perpendicular to the sliding direction. In our case, the scratch marks do not present any cracks at the macro or microscale. Regarding the end of the scratch marks, high-stress concentration appears behind the indenter tip, which causes angular microcracks. The layer deforms plastically. Local compressive stress is released once the indenter has passed. Material spallation failure initiates with the formation of compressive shear cracks ahead of the indenter. These cracks have sloping sides that act as a wedge. This facilitates propagation due to indenter movement. Because of this, the severity increases, which causes the wedge to lift the layer further. At the scratch mark end, as shown in Figure 16, rough spallation originates, and, at some point during indenter displacement, a microcrack is formed below the surface. This microcrack propagates to either side of the track and beyond, causing large areas of material displacement [19]. However, for the sample nitrided with a grid, the maximum displacement is higher. Still, no cracks appeared on the surface of the scratch mark or near it, as shown in Figure 16a, which means that the nitrided metal material has satisfactory properties for processing or stressing, at least concerning the test parameters presented.

Chemical composition (Table 10) using point mode was determined as in Figure 16a to follow the determination of the main element components and the evolution of N percentages between the surface percentage: points 1 and 6, scratch mark percentages at the beginning of the mark; points 3 and 5, at the end (the mark is deeper); points 2 and 4, with and without grid nitrided samples.

Determining chemical compositions through energy dispersive spectroscopy is mainly a qualitative investigation but can be used as a quantitative technique to compare the results between similar areas and investigation parameters. The chemical composition determinations confirm the indentation and scratch results mentioning that a higher percentage of nitrogen in the material leads to the formation of a larger number of harder compounds, the hardness will increase, and the coefficient of friction will decrease. A decrease of N percentage can be observed between the surface and the interior of the sample as the scratch advances in the material and its depth increases.

**Table 10.** Chemical composition of the areas selected in Figure 3a in wt and at%.

Elements/ Areas from Figure 3	N	
	at%	wt%
Pct1 (with)	14.96	12.20
Pct2 (with)	13.89	11.19
Pct3 (with)	12.91	11.36
Point 4	15.24	13.1
Point 5	13.67	11.44
Point 6	15.64	13.31
EDS det. error %		1.1

#### 4. Conclusions

In the situation of prismatic parts with angles of 30, 60, and 90, a comparison of the results from the two approaches (classical and polarized screen) during ionic nitriding produced the findings detailed below.

Concerning the cross-sectional analysis of the nitrided sample with a polarized screen, a relatively uniform diffusion layer can be observed from the SEM photographs, even on the sharp areas, which appear at the edges of the parts.

Comparing Figures 12 and 13, it is easy to see that the polarized screen makes it easier to obtain a smooth, uniform surface without oxides, adhesions, and burns, which ensures low roughness and good surface quality.

Nitrided steel samples show different degrees of wetting depending on the test liquids. In the case of distilled water and ethylene glycol, two polar liquids, poor wetting of the surfaces was observed. However, things were different for the coolant and the anti-friction oil, which presented oleophilic behavior. Coolant behaves differently in terms of surface wettability compared to the other test media. The explanation was attributed to the different balance of cohesive forces of the liquid itself and the forces exerted between the liquid and the substrate. On the other hand, a correlation between surface wettability and surface roughness was highlighted.

The sample nitrided without a grid presented higher hardness and indentation of Young's elastic module compared to the sample nitrided with a grid. The surface nitrided with the grid was smoother, free of debris, and more homogeneous regarding its mechanical properties. Even though the contact depth was almost twice as big, the sample nitrided with the grid still did not present cracks, pores, or defects of the scratch surface, confirming the good tenacity of the metallic material after the chemical treatment was applied. The nitrogen percentage varied between the surface and the scratch mark, confirming the diffusion of nitrogen in the metallic material.

**Author Contributions:** Conceptualization, writing, and investigation: M.A. and N.C.; Writing the original draft, project administration, and scientific supervision: C.N. and P.V.; Methodology, investigation, data curation, and validation: E.-L.E., M.A. and C.N.; Data curation, validation, and writing—reviewing and editing: D.-P.B.-N.; Resources and formal analysis: D.-P.B.-N. All authors have read and agreed to the published version of the manuscript.

**Funding:** This research received no external funding.

**Institutional Review Board Statement:** Not applicable.

**Informed Consent Statement:** Not applicable.

**Data Availability Statement:** Not applicable.

**Acknowledgments:** This work was supported by a research grant of the TUIASI, project number PN-III-27PFE/2021, COMPETE 2.0, financed by the Romanian Government, and in accordance with the proposals of the Representative of the Government of Romania.

**Conflicts of Interest:** The authors declare no conflict of interest.



## References

1. Braz, J.K.F.S.; Martins, G.M.; Sabino, V.; Vitoriano, J.O.; Barboza, C.A.G.; Soares, A.K.M.C.; Rocha, H.A.O.; Oliveira, M.F.; Alves Júnior, C.; Moura, C.E.B. Plasma Nitriding under Low Temperature Improves the Endothelial Cell Biocompatibility of 316L Stainless Steel. *Biotechnol. Lett.* **2019**, *41*, 503–510. [[CrossRef](#)] [[PubMed](#)]
2. Moldovan, E.R.; Doria, C.C.; Ocaña, J.L.; Istrate, B.; Cimpoesu, N.; Baltas, L.S.; Stanciu, E.M.; Croitoru, C.; Pascu, A.; Munteanu, C.; et al. Morphological Analysis of Laser Surface Texturing Effect on AISI 430 Stainless Steel. *Materials* **2022**, *15*, 4580. [[CrossRef](#)] [[PubMed](#)]
3. Saeed, A.; Khan, A.W.; Jan, F.; Abrar, M.; Khalid, M.; Zakaullah, M. Validity of “Sputtering and Re-Condensation” Model in Active Screen Cage Plasma Nitriding Process. *Appl. Surf. Sci.* **2013**, *273*, 173–178. [[CrossRef](#)]
4. Hassani-Gangaraj, S.M.; Guagliano, M. Microstructural Evolution during Nitriding, Finite Element Simulation and Experimental Assessment. *Appl. Surf. Sci.* **2013**, *271*, 156–163. [[CrossRef](#)]
5. Haftlang, F.; Habibolahzadeh, A.; Sohi, M.H. Improving Electrochemical Properties of AISI 1045 Steels by Duplex Surface Treatment of Plasma Nitriding and Aluminizing. *Appl. Surf. Sci.* **2015**, *329*, 240–247. [[CrossRef](#)]
6. Wang, S.; Cai, W.; Li, J.; Wei, W.; Hu, J. A Novel Rapid D.C. Plasma Nitriding at Low Gas Pressure for 304 Austenitic Stainless Steel. *Mater. Lett.* **2013**, *105*, 47–49. [[CrossRef](#)]
7. Hosseini, S.R.; Ashrafizadeh, F. Accurate Measurement and Evaluation of the Nitrogen Depth Profile in Plasma Nitrided Iron. *Vacuum* **2009**, *83*, 1174–1178. [[CrossRef](#)]
8. Asadi, Z.S.; Mahboubi, F. Effect of Component’s Geometry on the Plasma Nitriding Behavior of AISI 4340 Steel. *Mater. Des.* **2012**, *34*, 516–521. [[CrossRef](#)]
9. Allenstein, A.N.; Lepienski, C.M.; Buschinelli, A.J.A.; Brunatto, S.F. Plasma Nitriding Using High H<sub>2</sub> Content Gas Mixtures for a Cavitation Erosion Resistant Steel. *Appl. Surf. Sci.* **2013**, *277*, 15–24. [[CrossRef](#)]
10. Shen, L.; Wang, L.; Xu, J.J. Plasma Nitriding of AISI 304 Austenitic Stainless Steel Assisted with Hollow Cathode Effect. *Surf. Coat. Technol.* **2013**, *228*, S456–S459. [[CrossRef](#)]
11. Alphonsa, J.; Padsala, B.A.; Chauhan, B.J.; Jhala, G.; Rayjada, P.A.; Chauhan, N.; Soman, S.N.; Raole, P.M. Plasma Nitriding on Welded Joints of AISI 304 Stainless Steel. *Surf. Coat. Technol.* **2013**, *228*, S306–S311. [[CrossRef](#)]
12. Naeem, M.; Shafiq, M.; Zaka-ul-Islam, M.; Nawaz, N.; Díaz-Guillén, J.C.; Zakaullah, M. Effect of Cathodic Cage Size on Plasma Nitriding of AISI 304 Steel. *Mater. Lett.* **2016**, *181*, 78–81. [[CrossRef](#)]
13. Jasinski, J.J.; Fraczek, T.; Kurpaska, L.; Lubas, M.; Sitarz, M. Investigation of Nitrogen Transport in Active Screen Plasma Nitriding Processes-Uphill Diffusion Effect. *JMoSt* **2018**, *1164*, 37–44. [[CrossRef](#)]
14. Braceras, I.; Ibáñez, I.; Dominguez-Meister, S.; Sánchez-García, J.A.; Brizuela, M.; Larrañaga, A.; Garmendia, I. Plasma Nitriding of the Inner Surface of Stainless Steel Tubes. *Surf. Coat. Technol.* **2018**, *355*, 116–122. [[CrossRef](#)]
15. Kajzer, A.; Ceglarska, M.; Sura, N.; Kajzer, W.; Borowski, T.; Tarnowski, M.; Pilecki, Z. Effect of Nitrided and Nitrocarburised Austenite on Pitting and Crevice Corrosion Resistance of 316LVM Steel Implants. *Materials* **2020**, *13*, 5484. [[CrossRef](#)] [[PubMed](#)]
16. Borgioli, F.; Galvanetto, E.; Bacci, T. Effects of Surface Modification by Means of Low-Temperature Plasma Nitriding on Wetting and Corrosion Behavior of Austenitic Stainless Steel. *Coatings* **2020**, *10*, 98. [[CrossRef](#)]
17. Manfrinato, M.D.; de Almeida, L.S.; Rossino, L.S.; Kliauga, A.M.; Melo-Máximo, L.; Melo-Máximo, D.V.; Morón, R.C. Scratch Testing of Plasma Nitrided and Nitrocarburized AISI 321 Steel: Influence of the Treatment Temperature. *Mater. Lett.* **2022**, *317*, 132083. [[CrossRef](#)]
18. Kamminga, J.D.; Alkemade, P.F.A.; Janssen, G.C.A.M. Scratch Test Analysis of Coated and Uncoated Nitrided Steel. *Surf. Coat. Technol.* **2004**, *177–178*, 284–288. [[CrossRef](#)]
19. Laukkanen, A.; Holmberg, K.; Koskinen, J.; Ronkainen, H.; Wallin, K.; Varjus, S. Tribological Contact Analysis of a Rigid Ball Sliding on a Hard Coated Surface, Part III: Fracture Toughness Calculation and Influence of Residual Stresses. *Surf. Coat. Technol.* **2006**, *200*, 3824–3844. [[CrossRef](#)]

**Disclaimer/Publisher’s Note:** The statements, opinions and data contained in all publications are solely those of the individual author(s) and contributor(s) and not of MDPI and/or the editor(s). MDPI and/or the editor(s) disclaim responsibility for any injury to people or property resulting from any ideas, methods, instructions or products referred to in the content.